Influences of Various Supports, γ-Al$_2$O$_3$, CeO$_2$, and SBA-15 on HDO Performance of NiMo Catalyst

Binh M. Q. Phan · Quan L. M. Ha · Nguyen P. Le ·
Phuong T. Ngo · Thu H. Nguyen · Tung T. Dang ·
Luong H. Nguyen · Duc A. Nguyen · Loc C. Luu

Abstract Hydrodeoxygenation (HDO) of guaiacol
(GUA), has been carried out over γ-Al$_2$O$_3$, CeO$_2$, SBA-15
supported NiMo catalysts in an autoclave at 250 °C and a
hydrogen pressure of 5 MPa. In comparison with NiMo/γ-
Al$_2$O$_3$, both NiMo/CeO$_2$ and NiMo/SBA-15 catalysts
showed their higher activities. NiMo/SBA-15 has been
found to be the most potential one for HDO of GUA with
GUA conversion and HDO degree of 90 and 67.5 %,
respectively. The main product was cyclohexane with its
yield of 56 mol%. The outstanding activity of this catalyst
results from a high dispersion of its active sites on SBA-15
as catalyst support. For CeO$_2$ supported catalyst, some
interactions of Ce–Mo can be occurred, leading to an
enhancement of its HDO performance.

Keywords Hydrodeoxygenation · Guaiacol · γ-Al$_2$O$_3$ ·
CeO$_2$ · SBA-15 · NiMo-base catalyst

1 Introduction

Fast pyrolysis technology is commonly used for biomass
conversion into bio-oil, which is considered as a source of
alternative fuels [1]. Bio-oil is a complex mixture of
organic chemicals with high oxygen content and it is
necessary to remove oxygen from bio-oil to stabilize its
composition and improve its quality [2]. Recently, studies
of bio-oil upgrading were usually conducted with hydro-
deoxygenation (HDO) reaction, which can be applied to
fully remove oxygen from bio-oil [3]. Therefore, HDO can
be used at various levels to deeply upgrade bio-oil for
alternative fuel [4] or refinery feed blending purposes [5].

One of the typical supports for HDO catalyst is alumina.
However, in bio-oil HDO process, there are some main
drawbacks associated with boehmite formation due to the
presence of large amounts of water as well as the occur-
rence of potential carbon precursors during reaction [6–8].
The aim of this work is to determine the influences of
various supports, γ-Al$_2$O$_3$, CeO$_2$, and SBA-15 on HDO
performance of NiMo catalyst. SBA-15 is well known for
its high surface areas (up to 1000 m^2/g), which can
improve metal dispersion [9, 10]. Ceria is claimed to
improve the oxycompound activation, with the formation
of intermetallic M–Ce bonds [3, 11]. The catalytic per-
formance was determined on guaiacol (GUA), which is a
common model compound of bio-oil [12–14]. Up to now,
there have been studies of CeO$_2$ and SBA-15 as catalyst
supports for HDO of similar model compounds but with
different catalyst formulations [3, 11, 15, 16].

2 Experimental

2.1 Catalyst Preparation

Chemical compositions of supported Mo and NiMo cata-
lysts are listed in Table 1. All the catalysts used in this
work were prepared by impregnation method. The γ-Al$_2$O$_3$
was obtained from Merck. CeO$_2$ was produced by

B. M. Q. Phan · Q. L. M. Ha · N. P. Le (✉) ·
P. T. Ngo · T. H. Nguyen · T. T. Dang ·
L. H. Nguyen · D. A. Nguyen
Petrovietnam R&D Center for Petroleum Processing (PVPro),
Vietnam Petroleum Institute (VPI), 4 Nguyen Thong, District 3,
Ho Chi Minh City, Vietnam
e-mail: nguyenlp@pvpro.com.vn

L. C. Luu
Hochiminh City University of Technology, 268 Ly Thuong Kiet,
District 10, Ho Chi Minh City, Vietnam

Table 1 Chemical composition of studied catalysts

Composition (wt%)					Catalyst
NiO	MoO₃	γ-Al₂O₃	CeO₂	SBA-15	
6	30	64	–	–	NiMo/Al₂O₃
6	30	–	64	–	NiMo/CeO₂
6	30	–	–	64	NiMo/SBA-15
–	30	–	–	70	Mo/SBA-15

Table 2 BET surface area and pores volume (PV) of supports and NiMo catalysts

	BET ($m^2\ g^{-1}$)	PV ($cm^3\ g^{-1}$)
γ-Al₂O₃	132	0.25
CeO₂	83	0.24
SBA-15	853	0.88
NiMo/γ-Al₂O₃	86	0.17
NiMo/CeO₂	27	0.11
NiMo/SBA-15	270	0.52

calcining $Ce(NO_3)_3 \cdot 6H_2O$ (Sigma Aldrich) at 500 °C for 3 h. The SBA-15 was prepared by following a defined process [17]. The $(NH_4)_6Mo_7O_{24} \cdot 4H_2O$ (Sigma Aldrich) and $Ni(NO_3)_2 \cdot 6H_2O$ (Sigma Aldrich) chemicals, were used as Mo, Ni precursors, respectively. Solutions of precursors were prepared and then impregnated onto supports under stirring at 60 °C until all water vaporized. Samples were then dried at 110 °C and calcined in air at 500 °C for 3 h. Prior to reaction tests, catalysts were pre-treated with hydrogen in a batch reactor at 350 °C and 1 MPa for 1 h.

2.2 Catalyst Characterizations

Surface areas (SA) and pore volumes (PV) of the supports and catalysts were determined from nitrogen isotherms at −196 °C on a TRISTAR 3020 Micromeritics apparatus. Prior to measurements, samples were degassed at 260 °C in N_2 flow for 4 h. XRD patterns were recorded in the $20^o \leq 2\theta \leq 70^o$ range on a Bruker D8 Advance diffractometer using scintillation counter detector, equipped with a CuK radiation source. Small-angle XRD ($2\theta = 0.5^o - 10^o$) was performed on a Bruker D8 Advance diffractometer using lynxeye detector. TPR experiments were carried out in an AMI—902 (Altamira) automatic analyzer equipped with a TCD detector. Prior to the TPR test, samples were pre-treated in situ under Ar at 400 °C for 30 min and cooled to room temperature. The reduction step was performed with an mixture containing 10 % H_2 in Ar, by a heating rate of 10 K/min, up to 1000 °C. TEM images were obtained on a JEM-1010 (JEOL) transmission electron microscope with a magnification range of ×50–x500 K and an accelerating voltage range of 40–100 kV.

2.3 HDO Measurements

In a typical test, 40 g of 3 wt% GUA in n-hexadecane and 2 g catalyst were loaded into an autoclave reactor (Parr Instruments). The reactor was flushed with nitrogen, pressurized with H_2 (99.999 %) to 5 MPa at room temperature, and then heated to 250 °C. The starting time ($t = 0$) was recorded when the required reaction temperature was reached (250 °C), while stirring speed was set at 1000 rpm.

After 3-hour reaction, the reactor was cooled to room temperature. The gas was analyzed by gas chromatography (GC, HP 5890). The liquid products were analyzed by GCMS (Agilent 7890A Gas Chromatography, 5975C Mass Selective Detector).

Catalyst activity was estimated according to GUA conversion X_{GUA} (%) and HDO degree (%), which were calculated as follows [18]:

$$X_{GUA}(\%) = \frac{n_{GUA}^0 - n_{GUA}^{final}}{n_{GUA}^0}$$

$$HDO(\%) = \frac{n_{GUA}^0 \times X \times 2 - \sum_i n_i a_i}{n_{GUA}^0 \times X \times 2} \times 100\%$$
$$= \left(1 - \frac{\sum_i n_i a_i}{n_{GUA}^0 \times X \times 2}\right) \times 100\%$$

where, n_{GUA}^0 and n_{GUA}^{final} are initial and final amount of GUA (mol), respectively, n_i is amount of i-product (mol) in the liquid phase (except for unreacted GUA), a_i is number of oxygen atoms in the molecule of i-product.

The product distribution was calculated as follows [18]:

$$\varphi_i(\%) = \frac{n_i}{\sum_{i=j}^{k} n_i} \times 100$$

where $\varphi_i(\%)$ is molar fraction of i-product in the liquid phase, taking into account unreacted GUA.

The coke deposition on the catalysts was also evaluated with a Leco CS-600 analyzer after 3 h of reaction time.

3 Results and Discussions

3.1 Characterization of Catalysts

The surface area and pore volume (V_p) of the studied samples are given in Table 2. The SBA-15 possess a very large surface area therefore the active phase NiMo is supposed to be better dispersed on SBA-15 than alumina or ceria. Compared with supports, addition of NiMo (36 wt%)

Fig. 1 X-ray diffraction diffractograms of NiMo catalysts (a) and low angle X-ray diffraction diffractograms of SBA-15 and NiMo/SBA-15 catalyst (b)
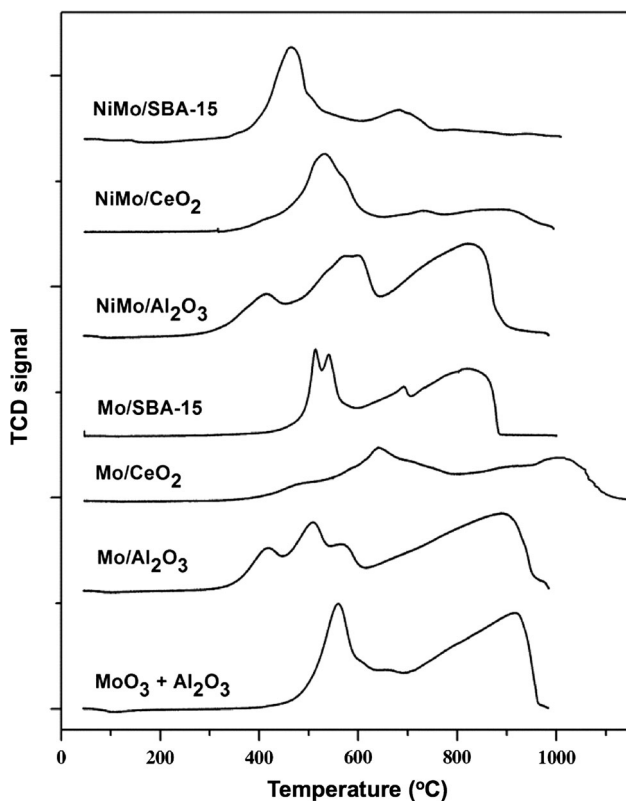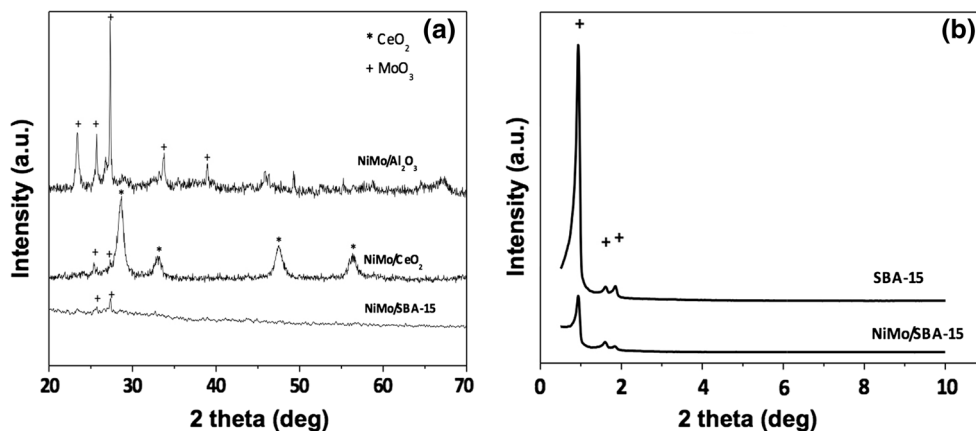

Fig. 2 TPR profiles of studied catalysts

leads to a significant decrease of BET surface area as well as V_p. It can be attributed to the coverage of active phase as well as the blockage of support pores. NiMo/SBA-15 exhibits the higher BET surface area, with 270, versus 86 m²/g and 27 m²/g for NiMo/Al₂O₃ and NiMo/CeO₂, respectively.

Figure 1a presents XRD diffractograms of NiMo catalysts. XRD peaks assignable to MoO_3 were detected for all the samples. However, the intensities of MoO_3 diffraction peaks ($2\theta = 23.4°$; $25.7°$; $27.4°$; $33.6°$ and $39.1°$) are quite lower in cases of NiMo/CeO₂ and NiMo/SBA-15. It can be attributed to a lower crystallinity of MoO_3 or a smaller crystalline size of MoO_3. In NiMo/CeO₂, the most peaks belong to CeO₂ crystalline phase.

Low angle XRD diffractograms for SBA-15 and NiMo/SBA-15 are shown in Fig. 1b. The peaks at 2θ of 0.84°, 1.45° and 1.68° show that a two dimensional hexagonal SBA-15 was prepared successfully and still remained in NiMo/SBA-15 catalyst. It is worthy to note that in all of these XRD diffractograms, there are no peaks associated with oxide of Ni, suggesting the existence of very small Ni grains [19, 20].

TPR profiles of Mo and NiMo based catalysts are shown in Fig. 2. In order to have a better understanding of the Mo-support interaction, a mechanical mixture of MoO_3 and γ-Al₂O₃, which is supposed to have no Mo-support interaction, is also studied. TPR profile of this sample exhibits two main peaks, one at 554 °C and the other at 910 °C, as well as a shoulder around 670 °C. The low-temperature (LT) peak can be assigned to a partial reduction step of Molybdenum trioxide ($Mo^{6+} \rightarrow Mo^{4+}$) of amorphous, multilayered Mo oxides or octahedral Mo species [21]. The high-temperature (HT) peak at 910 °C is ascribed to a deep reduction of all Mo species including less reducible tetrahedral Mo species, bulk MoO_3 or the reduction of isolated tetrahedral Mo^{6+} species in strong interaction with the support [22, 23]. The shoulder at 670 °C may be due to the intermediate-reducible of orthorhombic MoO_3 [24, 25].

TPR profile of Mo/Al₂O₃ shows two more peaks at LT region, one at 400 °C and the other at 500 °C. Those peaks can be assigned to the reduction of polymeric octahedral Mo species, which were more reducible than MoO_3 bulk species [21, 22, 26, 27]. Comparing to TPR profile of mechanical mixture of MoO_3 and γ-Al₂O₃, the HT peak shifted to 900 °C. For Mo/SBA-15, this HT peak even shifted to lower temperature (850 °C). On the contrary, with Mo/CeO₂ sample, the LT reduction peak moved to higher temperature at 620 °C and the HT one became a very broad peak completed beyond 1000 °C. Thus, it can
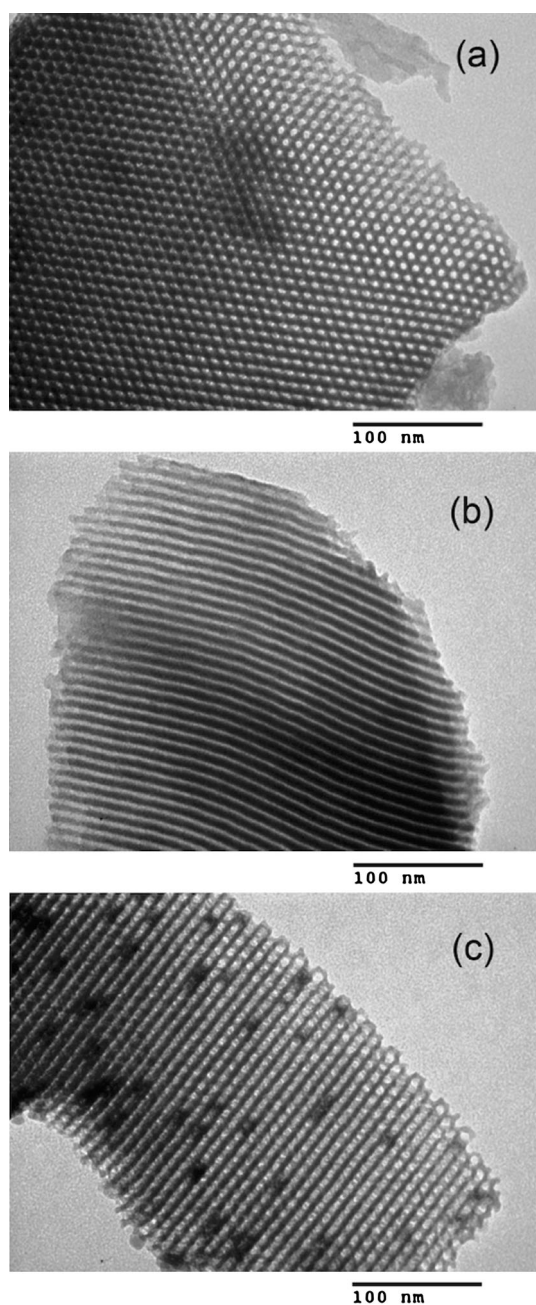
Fig. 3 Transmission electron microscopy images of (**a**), **b** SBA-15 support and **c** NiMo/SBA-15 catalyst

be suggested that the interaction between Mo species and CeO$_2$ support is stronger than that between Mo species and alumina or SBA-15. Then, even if X-ray diffraction does not evidence the presence of Mo–Ce mixed oxides species, interactions between these two compounds can not be excluded.

After the addition of Ni, the reduction of Mo species generally occurred at lower temperatures, indicating the promotional effect of Ni on Mo reduction [26, 28, 29]. Among NiMo catalysts, there are more easily reducible

Table 3 HDO performance and coke deposition of catalysts at 250 °C, 5 MPa and 3 h

	NiMo/ Al$_2$O$_3$	NiMo/ CeO$_2$	NiMo/ SBA-15	Mo/ SBA-15
X_{GUA} (%)	15.0	23.0	90.0	7.0
HDO (%)	18.5	20.0	67.5	26.0
Coke deposition (wt%)	2.3	0.7	2.6	0.9
Product				
Non-oxygen compounds				
Methylcyclopentane	–	–	0.6	–
Cyclohexane	–	5.0	55.8	–
Methylcyclohexane	–	–	2.1	–
1,1′-Bicyclohexyl	–	–	1.3	–
1-Oxygen compounds				
Cyclopentanemethanol	–	1.3	4.1	–
Cyclohexanol	–	27.1	6.3	–
Methoxycyclohexane	–	–	4.7	–
Cyclohexanone	–	–	–	5.3
Phenol	32.5	0.8	–	41.0
p-Cresol	4.5	–	–	5.6
2-Oxygen compounds				
1,2-Cyclohexanediol	–	4.2	–	–
2-Methoxycyclohexanol	–	43.0	6.7	–
1,2-Dimethoxycyclohexane	–	–	12.6	–
1,2-Dimethoxybenzene	51.8	16.8	5.8	45.0
3-Methylmequinol	–	1.8	–	–
Methyl GUA	11.2	–	–	3.1

species in NiMo/SBA-15. It can be seen in its TPR profile that Mo^{+6} species were reduced at 450 °C for the first step and 700 °C for the complete step, which were both similarly reported in another study [28].

Regarding the HT peaks of all samples, the use of SBA-15 as a support for NiMo catalyst can limit the formation of MoO$_3$ bulk species or isolated tetrahedral Mo^{6+} species in strong interaction with the support. Consequently, MoO$_3$ can be well dispersed on the surface of SBA-15. The better dispersion of MoO$_3$ species on SBA-15 can also be seen on TEM images (Fig. 3) and XRD patterns where intensities of the characteristic XRD signals of MoO$_3$ of NiMo/SBA-15 were much lower than those of NiMo/Al$_2$O$_3$ and NiMo/CeO$_2$ (Fig. 1a).

Figure 3 shows TEM micrographs of SBA-15 support and NiMo/SBA-15 catalyst. The TEM analysis of SBA-15 (Fig. 3a, b) indicates that a well-ordered hexagonal array of mesopores can be observed when electron beam was parallel to the main axis of cylindrical pores. When electron beam is perpendicular to the main axis, cylindrical pores are viewed from the side as a striped image. Distance between centers of two adjacent pores was about 10 nm, and their pore diameters were about 6 nm. On NiMo/

SBA-15 TEM image (Fig. 3c), it can be seen that active phase is well dispersed on the support with the average diameter of the mean particle size about 5 nm.

3.2 HDO Measurements

Table 3 shows catalytic activity tests of NiMo based catalysts with GUA as feed at 250 °C, 5 MPa. In the blank test without catalyst, no GUA conversion is observed under the reaction conditions. The standard deviations of repetition are all below 10 %, indicating an acceptable repeatability for HDO degree. The metal leaching was also examined by ICP after 3 h of reaction time. Only trace amounts of Mo and/or Ni (<100 ppm) are found in the leaching solution. In all experiments, the gas obtained contained mainly unreacted H_2, with minor amounts of methane. Hence, comparison of the catalysts was based on liquid products only. These products were homogeneous in our experiments, and no phase separation was detected in any sampling and analyzing processes.

Comparing to $NiMo/Al_2O_3$ as reference catalyst, both $NiMo/CeO_2$ and NiMo/SBA-15 exhibit higher performances in HDO reaction of GUA. Furthermore, NiMo/SBA-15 is found as the most effective catalyst that gives more than 90 % of GUA conversion and 67.5 % of HDO degree at 250 °C.

For the $NiMo/Al_2O_3$ catalyst, liquid products contain mainly 1,2-dimethoxybenzene (51.8 mol%) and main deoxygenated product is phenol. Also, no saturated ring is detected in the product. The high yield of phenol is attributed to the reaction route proposed in literature with NiMo and CoMo based catalysts [12, 30, 31], where the GUA tranformation is found to initialize with the demethylation (DME) and/or demethoxylation (DMO) step to form catechol and/or phenol.

Compared to $NiMo/Al_2O_3$, the use of CeO_2 as catalyst support results in a slight increase in catalyst performance as well as in products distribution despite its lower surface area (Table 2). 2-methoxycyclohexanol is detected with highest yield (43.0 mol%) for $NiMo/CeO_2$. Cyclohexanol (27.1 mol%) is observed as the highest deoxygenated product as well as cyclohexane is also observed in the product mixture. Then, the higher activity of $NiMo/CeO_2$ compared with that of $NiMo/Al_2O_3$ can be attributed to the strong interaction between Mo species and ceria even if this parameter should be not the only one (Figs. 1, 2). Besides, the high yield of 2-methoxycyclohexanol shows the benzene ring hydrogenation promotion effect of the Ni supported on ceria catalyst. This result is in accordance with the study of Barrault [29]. They have proposed the high hydrogenation activity of Ni–Ce catalyst resulted from the synergy effect of Ni and Ce.

For the NiMo/SBA-15 catalyst, a high surface area of SBA-15 leads to a better active phase dispersion, which can be observed on TEM images and TPR profiles (Figs. 2, 3). This result seems to indicate a higher GUA conversion performance compared with $NiMo/Al_2O_3$ and $NiMo/CeO_2$ catalysts. Then, about 95 mol% of the products contained no benzene ring, nearly 60 mol% of those contained no oxygen and other 15 mol% of those contained only one oxygen atom in their molecules. Moreover, well-dispersed Ni can play a key role in GUA conversion and HDO performance since the activity of Mo/SBA-15 catalyst is much lower than NiMo/SBA-15 catalyst (Table 3). Only 7 % of GUA is converted with Mo/SBA-15 and the main product is phenol. As the result, Ni can take part in HDO activity as proposed in other studies by increasing Mo dispersion [28, 32]. It can be further discussed about another possible pathway that well-dispersed Ni, through its ring hydrogenation activity, create high yield of saturated oxygenate compounds (Table 3) which were identified more reactive for hydrogenolysis reaction [3]. This pathway can be found in other study with the HDO reaction conducted with noble metal type catalyst [30].

As shown in Table 3, the ceria catalyst shows less coke deposition in comparison with any other catalysts of this study. CeO_2-based materials have been widely used as an oxygen storage material associated to the redox property of Ce [33]. Therefore, the use of ceria as support can effectively inhibit coke formation [34]. In addition, the considerably lower acidity of Ni/CeO_2 catalyst (results not shown) may also suppress the coke deposition [35].

4 Conclusions

In this study, the influences of different supports, γ-Al_2O_3, CeO_2, and SBA-15, on NiMo based catalyst for bio-oil HDO reaction was investigated. It can be pointed out that the beneficial effect of SBA-15 support for HDO performance is associated with the high dispersion of NiMo. NiMo/SBA-15 is a very promising catalyst for bio-oil HDO reaction with its GUA conversion of 90 % and HDO degree of 67.5 %. This catalyst also exhibits a significant hydrogenation promotion effect that created a high yield of cyclohexane and other saturated ring compounds. NiMo/CeO_2 also shows benzene hydrogenation promotion effect which enhanced formation of cyclohexane. As evidenced from TPR studies, interaction of Mo and CeO_2 which creates a new active phase probably promoting its hydrogenation acivity. The use of ceria as support also inhibits the coke formation as compared with alumina or SBA-15 based catalysts.

References

1. Lange JP (2007) Catalysis for renewables. Wiley-VCH Verlag GmbH & Co. KGaA, Weinheim
2. Mohan D, Pittman CU, Steele PH (2006) Energy Fuels 20:848–889
3. Mortensen PM, Grunwaldt JD, Jensen PA, Knudsen KG, Jensen AD (2011) Appl Catal A 407:1–19
4. Wildschut J, Mahfud FH, Venderbosch RH, Heeres HJ (2009) Ind Eng Chem Res 48:10324–10334
5. Bui VN, Toussaint G, Laurenti D, Mirodatos C, Geantet C (2009) Catal Today 143:172–178
6. Venderbosch RH, Ardiyanti AR, Wildschut J, Oasmaa A, Heeres HJ (2010) J Chem Technol Biotechnol 85:674–686
7. Elliott DC (2007) Energy Fuels 21:1792
8. Şenol Oİ, Viljava TR, Krause AOI (2005) Catal Today 106:186–189
9. Antonakou E, Lappas A, Nilsen MH, Bouzga A, Stöcker M (2006) Fuel 85:2202–2212
10. Huirache-Acuña R, Nava R, Peza-Ledesma C, Lara-Romero J, Alonso-Núez G, Pawelec B, Rivera-Muñoz E (2013) Materials 6:4139–4167
11. Trovarelli A (1996) Catal Rev 38:439
12. Bui VN, Laurenti D, Delichère P, Geantet C (2011) Appl Catal B 101:246–255
13. Zhao HY, Li D, Bui P, Oyama ST (2011) Appl Catal A 391:305–310
14. Gutierrez A, Kaila RK, Honkela ML, Slioor R, Krause AOI (2009) Catal Today 147:239–246
15. Boullosa-Eiras S, Lodeng R, Bergem H, Stocker M, Hannevold L, Blekkan EA (2014) Catalysis: vol 26. The Royal Society of, Chemistry, pp 29–71
16. He Z, Wang X (2012) Catal Sust Energy 1:28
17. Luan Z, Hartmann M, Zhao D, Zhou W, Kevan L (1999) Chem Mater 11:1621–1627
18. Bykova MV, Ermakov DY, Kaichev VV, Bulavchenko OA, Saraev AA, Lebedev MY, Yakovlev VA (2012) Appl Catal B 113–114:296–307
19. Alberton AL, Souza MMVM, Schmal M (2007) Catal Today 123:257–264
20. Jin S, Xiao Z, Li C, Chen X, Wang L, Xing J, Li W, Liang C (2014) Catal Today 234:125–132
21. Regalbuto J, Ha JW (1994) Catal Lett 29:189–207
22. Maity SK, Srinivas BN, Prasad VVDN, Singh A, Murali Dhar G, Rao TSRP (1998) Studies in surface science and catalysis. Elsevier, Amsterdam, pp 579–590
23. Chary KVR, Bhaskar T, Seela KK, Sri Lakshmi K, Reddy KR (2001) Appl Catal A 208:291–305
24. Rajagopal S, Marini HJ, Marzari JA, Miranda R (1994) J Catal 147:417–428
25. Marzari JA, Rajagopal S, Miranda R (1995) J Catal 156:255–264
26. Brito J, Laine J (1986) Polyhedron 5:179–182
27. Ramírez J, Macías G, Cedeño L, Gutiérrez-Alejandre A, Cuevas R, Castillo P (2004) Catal Today 98:19–30
28. Gutiérrez OY, Valencia D, Fuentes GA, Klimova T (2007) J Catal 249:140–153
29. Barrault J, Alouche A, Paul-Boncour V, Hilaire L, Percheron-Guegan A (1989) Appl Catal 46:269–279
30. Lin Y-C, Li C-L, Wan H-P, Lee H-T, Liu C-F (2011) Energy Fuels 25:890–896
31. Bui VN, Laurenti D, Afanasiev P, Geantet C (2011) Appl Catal B 101:239–245
32. Romero Y, Richard F, Brunet S (2010) Appl Catal B 98:213–223
33. Roh HS, Eum IH, Jeong DW (2012) Renew Energy 42:212–216
34. Lin KH, Tsai CY, Chang ACC (2013) Mod Res Catal 2:42–49
35. Furimsky E, Massoth FE (1999) Catal Today 52:381–495